Supporting information for

Characterization of a Paramagnetic Mononuclear Nonheme Iron-Superoxo Complex

Chien-Wei Chiang,[†] Scott T. Kleespies,[‡] Heather D. Stout,[#] Katlyn K. Meier,[#] Po-Yi Li,[†] Emile L. Bominaar,[*,#] Lawrence Que, Jr.,[*,‡] Eckard Münck,[*,#] and Way-Zen Lee[*,†]

[†] *Department of Chemistry, National Taiwan Normal University, Taipei, 11677, Taiwan (R.O.C.);*

[‡] *Department of Chemistry and Center for Metals in Biocatalysis, University of Minnesota, Minneapolis, Minnesota 55455, United States;*

[#] *Department of Chemistry, Carnegie Mellon University, Pittsburgh, Pennsylvania 15213, United States*

Experimental Section

Materials and Methods. All manipulations were performed under nitrogen using standard Schlenk techniques. Acetonitrile was distilled once from P_2O_5 and freshly distilled from CaH_2 before use. Dichloromethane was distilled from CaH_2 before use. Diethyl ether and THF were dried by distillation from sodium benzophenone prior to use. All other chemicals were of analytical or spectroscopic grade and purchased from commercial sources and used without further purification. 2,6-Bis(((S)-2-(diphenylhydroxymethyl)-1-pyrrolidinyl)methyl)pyridine (H_2BDPP) and 9,10-dihydroanthracene-d_4 were synthesized according to literature procedures.[1]

[Fe^{II}(BDPP)] (**1**) was synthesized by reacting a mixture of NaH (0.0120 g, 0.5 mmol), H_2BDPP (0.1220 g, 0.2 mmol) and $FeCl_2$ (0.0253 g, 0.2 mmol) in 15 mL CH_3CN in a 100-mL Schlenk flask. The suspension solution was stirred at room temperature for 16 h and then filtered; the filtrate was concentrated under vacuum. Adding hexane (3 × 50 mL) to the concentrated filtrate resulted in the precipitation of a red residue of **1**. After filtration, the residue of **1** was dried under vacuum and redissolved in CH_2Cl_2 (10 mL). Complex **1** was then recrystallized by slow diffusion of pentane into the CH_2Cl_2 solution of **1** at room temperature. Red crystals of **1** were obtained over three days in 55% yield (0.7290 g). UV/vis (CH_3CN): 325 nm (1450 M^{-1} cm^{-1}), 530 nm (570 M^{-1} cm^{-1}). Anal. Calcd for [Fe(BDPP)]•0.5CH_2Cl_2 or $C_{41.5}H_{42}ClFeN_3O_2$: C, 70.59; H, 6.00; N, 5.95. Found: C, 70.93; H, 6.43; N, 5.97.

UV-vis spectra were recorded on Agilent 8453 diode-array spectrometer equipped with a cryostat from Unisoku Scientific Instruments, Osaka, Japan. Cyclic voltammetry measurements were performed by means of a three-electrode technique by using a home-built computer-controlled instrument on CH_2Cl_2 solutions containing 0.1M tetrabutylammonium tetrafluoroborate as electrolyte with Ag wire used as reference electrode and a glassy carbon electrode as the working electrode. The reported potentials were referenced with respect to the ferrocenium/ferrocene couple, which was recorded at the end of each experiment. NMR spectra were recorded on Bruker Avance-400 MHz FT NMR spectrometers. Elemental analyses for C,

H, and N were performed on a Perkin-Elmer 2400 analyzer at the NSC Regional Instrumental Center at National Taiwan University, Taipei, Taiwan.

Resonance Raman spectra were collected with 413.1-nm excitation from a Spectra-Physics model 2060 krypton-ion laser and an Acton AM-506 monochromator equipped with a Princeton LN/CCD data collection system. Spectra in THF and d_8-THF were obtained at 77 K using a 135° backscattering geometry. Samples were frozen onto a gold-plated copper cold finger in thermal contact with a Dewar flask containing liquid N_2. As the sample suffered photodegradation from laser irradiation, the laser beam was slowly scrolled over the frozen surface during data collection to present fresh spots for irradiation during the course of the experiment. Raman frequencies were calibrated to indene prior to data collection. The monochromator slit width was set for a band pass of 4 cm^{-1} for all spectra. Raman spectral intensities were calibrated relative to the 1145-cm^{-1} solvent peak of THF or the 962-cm^{-1} solvent peak of d_8-THF.

Mössbauer spectra were recorded with two spectrometers, using Janis Research Super-Varitemp dewars that allowed studies in applied magnetic fields up to 8.0 T in the temperature range from 1.5 to 200 K. Mössbauer spectral simulations were performed using the WMOSS software package (WEB Research, Edina, MN). Isomer shifts are quoted relative to Fe metal at 298 K.

For the X-ray structure determination, a crystal of **1** with a suitable size for CCD X-ray diffractometer was selected under a microscope and mounted on the tip of a glass fiber fashioned on a copper pin. X-ray data for complex **1** were collected on a Bruker Kappa APEX II CCD diffractometer employing graphite monochromated Mo Kα radiation (λ = 0.7107 Å) at 200 K and a θ - 2θ scan mode. The space group for complex **1** was determined on the basis of systematic absences and intensity statistics, and the structure of **1** was solved by direct methods using SIR92 or SIR97, and refined using SHELXL-97. An empirical absorption correction by multiscans was applied to the structure of **1**. All non-hydrogen atoms were refined with anisotropic displacement factors. H-atoms were placed in ideal positions and fixed with relative isotropic displacement parameters. Detailed crystallographic data of **1** are provided in a CIF file.

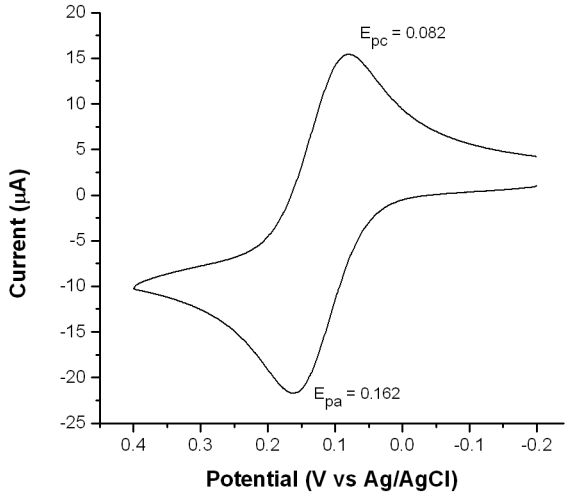

Figure S1. Cyclic voltammetry of **1** in CH_3CN

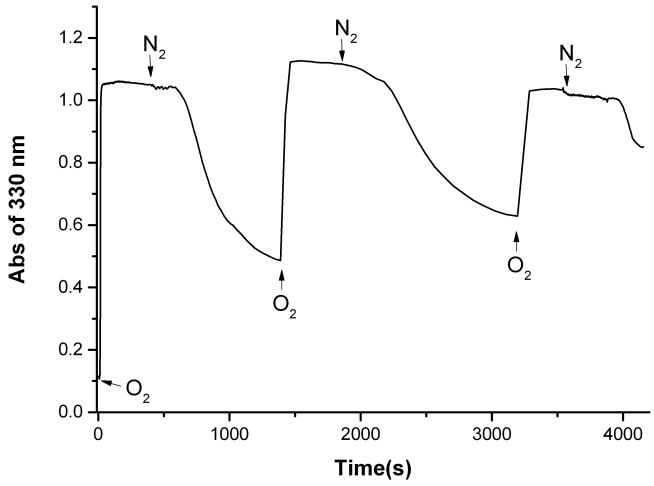

Figure S2. Time traces showing the reversible O_2 binding ability of **1** (0.2 mM) by alternately bubbling O_2 and N_2 into the THF solution at -80 °C.

Reactivity Studies and Product Analysis. The reaction of the iron(III)-superoxo complex **2**, [Fe(BDPP)(η^1-O_2^-)], and 9,10-dihydroanthracene (DHA) was monitored by UV-vis spectroscopy at -70 °C in THF (3.0 mL). Complex **2** was prepared by bubbling O_2 from a balloon into a solution of **1** for 1 min, and the increase of the absorption band at 330 nm due to the formation of **2** was monitored. DHA was then added to start the reaction with the *in situ* generated **2**. Reactions with different equivalents of DHA were carried out at least three times, and the average values of k_{obs} for different equivalents of DHA were plotted in Figure S3. Product analysis for the oxidation of DHA by **2** was performed by GC-MS, and the product yield was determined by comparing against the standard curves prepared from authentic samples.

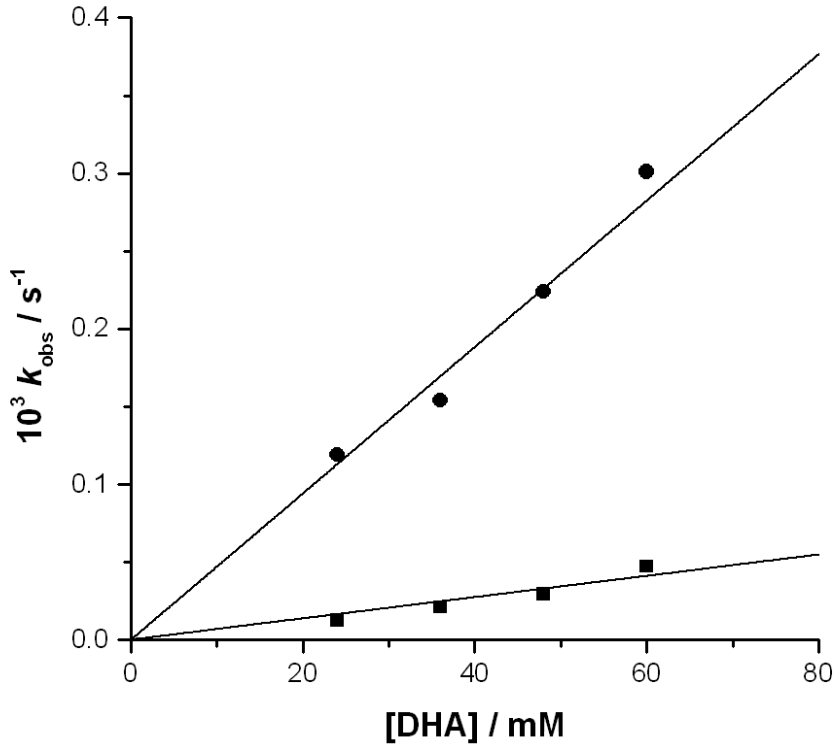

Figure S3. Plot of k_{obs} values versus substrate concentration for the reaction of 0.6 mM **2** with DHA (●) and DHA-d_4 (■). KIE = 7.

Comments on the Mössbauer spectra of 2

The space restrictions in the main manuscript did not allow us to comment on some aspects of our data analysis. The following comments should help to clarify a few points for the reader.

*Electron Spin Relaxation of **2***.

At 4.2 K the electronic spin of **2** relaxes slowly compared to the nuclear precession frequencies. In the slow relaxation regime of the electronic spin, each of the seven populated spin levels of the S = 3 ground multiplet contributes its own Mössbauer spectrum, with intensities governed by Boltzmann factors. Slow spin relaxation is evident from the observation that the B = 2.2 mT and 45 mT spectra display paramagnetic hyperfine structure. We do not show a Mössbauer spectrum recorded at T = 100 K, because at this temperature we observed an *asymmetric* quadrupole doublet with $\Delta E_Q \sim$ 1.6-1.8 mm/s, indicating that the relaxation is *approaching* the fast relaxation limit (At 4.2 K we obtained more precise values for ΔE_Q from the $M_S = \pm 2$ sublevel). A spectrum collected at 11 K and for B = 45 mT showed some broadening of the absorption lines, indicating that the spin system of **2** is making a transition to intermediate relaxation. As we pointed out in the main text, the 11 K spectrum hints at S = 3; however, given that we are not strictly in the slow relaxation limit, it is prudent to reserve final judgment until we obtain additional data. Switching solvent (especially to glassing solvents) for EPR and Mössbauer studies or diluting the sample may yield subtle changes, which allow us to conclusively determine the spin state of **2**.

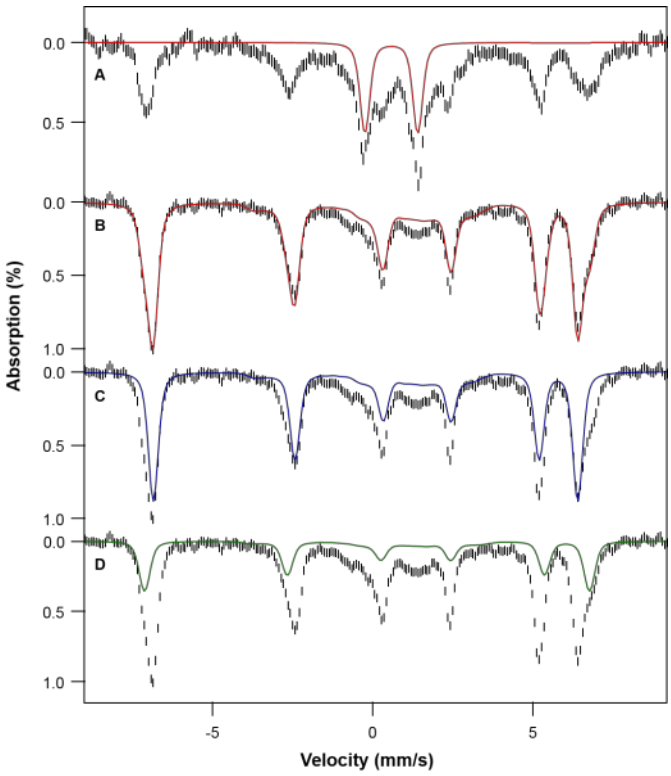

Figure S4. 4.2 K Mössbauer spectra of **2** recorded in zero-field (A) and in an applied field of B = 45 mT (B). Spectrum (B) is the same as that shown in Figure 4C. The red line in (A) outlines a quadrupole doublet that represents ≈ 10% of the Fe in the sample. The red line in (B) is a spectral simulation for **2** based on eq 1 and represents 89 % of the Fe; simulation parameters used are those listed in the caption of Fig. 4. The theoretical curves in (C) and (D) show the subspectra attributed to conformer **2a** (62%, blue) and **2b** (27%,green).

Comments on the zero field spectrum of **2**.

The zero field spectrum of Figure S4A (same spectrum as in Fig. 4A) contains a paramagnetic component similar to the one assigned to the $M_S = \pm 3$ doublet in Figure S4B (same spectrum as in Fig. 4C). For $\Delta_g >> |A_z|$ each level would contribute in zero applied field a quadrupole doublet with the same ΔE_Q; A_z, the z component of the ^{57}Fe magnetic hyperfine tensor, is the relevant quantity here (see Table 1 of ref 2). An exceedingly rare situation occurs when $|A_z| > \Delta_g$ (this is the case analyzed in ref 2). In this case the magnetic hyperfine interactions can mix the two

electronic levels of the $M_S = \pm 3$ doublet (called ψ^- doublet in eq 2 of ref 3) and the Mössbauer spectrum of the non-Kramers system displays magnetic hyperfine splittings even in zero field (see in particular Table 1 and Figure 2 of ref 2). For $6(g_z\beta B + A_z m_I) >> \Delta_g$ the two ψ^- levels change into the magnetic states |3,+3> and |3,-3> with expectation values $<S_z> = +3$ and $<S_z> = -3$, respectively, and we observe a 6-line Mössbauer patterns as shown in Figure 4B. (m_I is the nuclear magnetic quantum number.)

*Why do we use two similar species for **2** for the simulations?*

The 45 mT spectrum recorded at 4.2 K (Figures 4C and S4B) exhibits a shoulder on the high-energy line at + 7 mm/s Doppler velocity. We have explored the possibility that this shoulder represents the high-energy line of a mononuclear high-spin Fe^{III} contaminant. In fact, EPR spectra of a similar, but not parallel, preparation of **2** showed a signal at g = 4.3, corresponding to E/D ≈ 1/3. If such a contaminant were present in our Mössbauer sample, its ground Kramers doublet ($g_z \sim 9.7$, g_x, $g_y < 1$) would yield a 6-line spectrum with intensities 3:2:1:1:2:3 as observed for **2**. We have not found any line of this species other than the line forming the shoulder at +7 mm/s. This would imply that most of the spectrum of the contaminant hides under the lines of **2**. This would suggest that the putative contaminant has the same $B_{int} \sim -41$ T, $\delta \approx 0.58$ mm/s and quadrupole parameters as **2**, a rather implausible suggestion. We have therefore modeled the shoulder by assuming the presence of a slightly different form of **2**, called **2b** (representing 27% of Fe), as might be possible if a fraction of molecules had a slightly different orientation of the superoxo moiety. The major component, **2a**, accounts for 62% of the Fe present, so that **2a** and **2b** represents 89% of the Fe. The 2.2 mT spectrum (Figure 4B), especially the high energy feature, might also indicate the presence of two similar species.

Is there a contaminant?

The theoretical curve of Figure 4C is plotted to represent 89% of the Fe in the sample, suggesting that a species other than **2** might be present. There is some broad shallow absorption in the center

of the spectrum of Figure 4C. We currently do not know the nature of the species that gives rise to this absorption. Whatever this species might be, its presence will not affect the precision of the parameters obtained for **2**.

*Spectrum of **2** recorded for B = 3.0 T*

Figure S5 shows a Mössbauer spectrum of **2** recorded at 4.2 K for B = 3.0 T. The 3.0 T field mixes the electronic states of the S = 3 multiplet to a degree that depends on the magnitude of the zero field spitting parameter D. This mixing results in a ground state for which $\langle S_{x,}\rangle \approx -1.86$, $\langle S_y\rangle \approx -1.36$, and $\langle S_z\rangle = -3.0$, yielding an internal field $\mathbf{B}_{int} = -\langle \mathbf{S}\rangle \bullet \mathbf{A}/g_n\beta_n$ that is not uniaxial as it is at low field. Under these conditions the intensities of the nuclear $\Delta m_I = 0$ transitions (arrows in Figure S5) are reduced by an amount that depends on D {compare the intensities of the rightmost $\Delta m_I = 0$ line in Fig. S4A and Fig. S5}. The best simulation of the 3.0 T spectrum of Figure S5 yields D = -1.2 cm^{-1}.

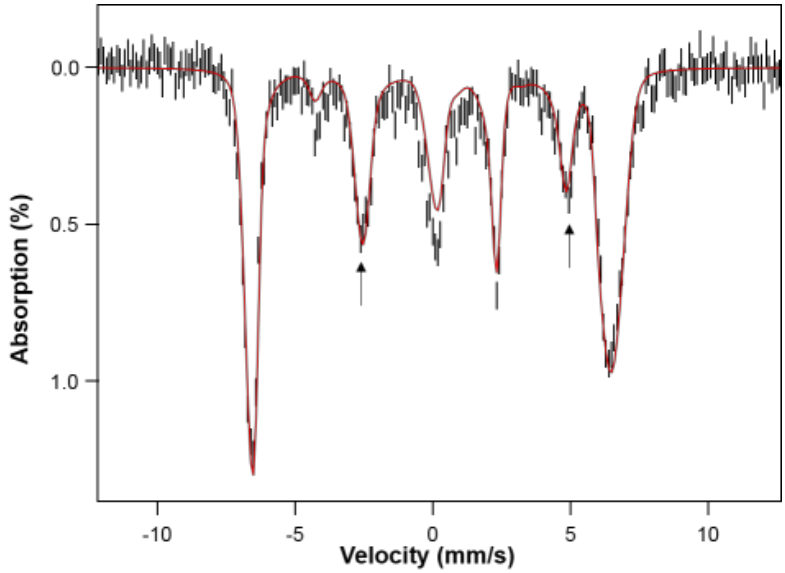

Figure S5. 4.2 K Mössbauer spectrum of **2** recorded in a 3.0 T field applied parallel to the observed γ rays. Arrows point at the nuclear $\Delta m_I = 0$ transitions. The red line is a simulation for an S = 3 spin Hamiltonian (eq 1 of the main text), using the parameters listed in the caption of Figure 4. In addition we used $A_{x,y}/g_n\beta_n = -16.5$ T for **2a** and -17.0 T for **2b**.

Why do the M_s = ±2 levels produce a quadrupole doublet for B = 2.2 mT ?

The quoted range of Δ_g values suggests E/D ≈ 0.08; if we take D = -1.2 cm^{-1} we obtain Δ_e ≈ 0.11 cm^{-1}. For this value of Δ_e the M_S = ±2 levels will yield a slightly broadened quadrupole doublet for B = 2.2 mT ($<S_z>_e$ = ± 0.14), whereas magnetic features would be observed at 45 mT when $<S_z>_e$ = ±1.63, a field for which the Zeeman term is sufficiently large to compete with Δ_e (see "magnetization" curves in Figure S6). E/D must be larger than zero because otherwise the M_S = ±2 doublet would exhibit paramagnetic hyperfine structure for B = 2. The M_S = ±1 levels a Δ value substantially larger than Δ_e and thus yield a quadrupole doublet; these levels, however, are barely populated at 4.2 K.

*Expectation values <**S**> for the M_S = ± 3 and ± 2 doublets.*

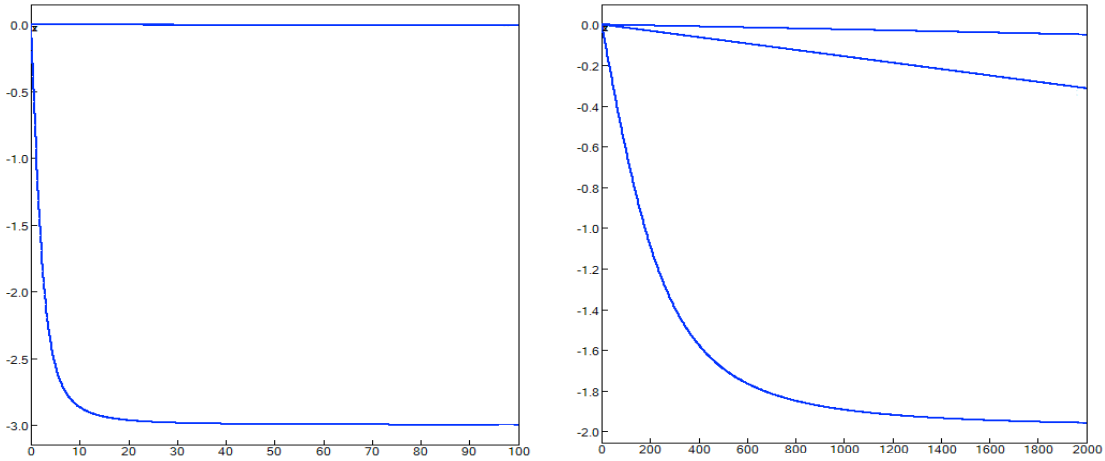

Figure S6. Plots of the expectation values of the electron spin. $<S_x>$ is the expectation value when the applied field B is along x. Field directions are labeled x,y, z. (A): Plot of $<S_i>$ for the M_S = -3 level. The M_S label is appropriate for B > 20 Gauss. (B) Plot of $<S_i>$ of the M_S = -2 level. Note that the expectation values for this doublet are very small for B = 2.2 mT (22 Gauss); that is the reason for the observation of a quadrupole doublet.

Mössbauer parameters obtained by assuming a ground state with S = 2.

The values for ΔE_Q, η, and δ are the same whether the data are analyzed for an S = 3 or an S = 2 multiplet. By assuming S = 2 we would obtain for the $M_S = \pm 2$ ground doublet $\Delta_g = 3D(E/D)^2 \approx$ 1-2 $\times 10^{-3}$ cm^{-1}. The D-value estimated from the 3.0 T spectrum would be $D(S = 2) \approx -2$ cm^{-1}, suggesting $(E/D) \approx 0.01$-0.02. These parameters would yield a parallel mode signal at $g \approx 8$; however, as the EPR intensity is proportional to $(E/D)^4$, the expected g = 8 signal would be 10,000 times weaker than that reported for the HPCD superoxo intermediate [3].

Analysis using an S = 2 Hamiltonian yields $A_z/g_n\beta_n = -20.6$ T for conformer **2a**. This parameter is related to the intrinsic parameter of the Fe^{III} site, $A_{z,1}$, by $A_z = (7/6)\ A_{z,1}$, which yields $A_{z,1} = -17.7$ T. From the S = 3 analysis we obtain $A_{z,1} = -(6/5)\ 13.8$ T $= -16.6$ T. (Determination of A_x and A_y requires further studies in strong applied fields, but $A_{x,y,1}/g_n\beta_n \approx -20$ T). At present, we cannot use these A_1-values to determine S because we lack information on typical A_1-values of (BDPP)Fe^{III} sites. A preliminary study of (BDPP)Fe^{III} in THF gave $A_1/g_n\beta_n \approx -(18$-$19)$ T, which is smaller than the typical -(21-22) T of octahedral Fe^{III} with N/O ligation , but is in the range of values observed here. However, even with such information available, the A_1-values would be too close to distinguish between S = 2 and S = 3. We are confident that we will obtain the desired information from Mössbauer or EPR, after some modification of solvent.

References

1. a) for BDPP: Zhang, Y.-X.; Du, D.-M.; Chen, X.; Lü, S.-F.; Hua, W.-T. *Tetrahedron: Asymmetry* **2004**, *15*, 177–182. b) for DHA-d_4: Goldsmith, C. R.; Jonas, R. T.; Stack, T. D. P. *J. Am. Chem. Soc.*, **2002**, *124*, 83-96.
2. Surerus, K. K.; Hendrich, M. P.; Christie, P. D.; Rottgardt, D.; Orme-Johnson, W. H.; Münck, E. *J. Am. Chem. Soc.* **1992**, *114*, 8579.
3. Mbughuni, M. M.; Chakrabarti, M.; Hayden, J. A.; Bominaar, E. L.; Hendrich, M. P.; Münck, E.; Lipscomb, J. D. *Proc. Natl. Acad. Sci. U.S.A.* **2010**, *107*, 16788